Actuation Requirements for Hopping and Running of the Musculoskeletal Robot BioBiped1

Katayon Radkhah[†] and Oskar von Stryk, *Member*, *IEEE*

Abstract— **Actuation with variable elasticity is considered a key property for the realization of human-like bipedal locomotion. Also, an intelligent and self-stable mechanical system is indispensable. While much effort of current research has been devoted to the development of variable impedance joint actuators, this paper deals with the important question of how to determine the actuation requirements of a compliant, musculoskeletal robot that is targeted at fast dynamic motions. In a step-by-step approach, design decisions for the elastic humanoid robot BioBiped1 are presented. Using multibody system dynamics models and simulations, incorporating bidirectional series elastic actuator models and a realistic ground contact model, we analyze the actuation requirements of the employed electrical motors for computer generated hopping and human data based running motions. The numerical simulation results are accompanied by videos of the dynamics simulations. Recent experiments on the real hardware have indicated that the selected motor-gear units and elastic transmissions support the desired dynamic motion goals.**

I. INTRODUCTION

Developing bipedal systems that are capable of fast and versatile motions represents a grand challenge for actuation and control. As surveyed in [1], [2], a variety of robotic actuation principles exists. Recent interest has centered on compliant actuator designs [3] and development of new variable impedance actuator concepts and prototypes for manipulation, locomotion and rehabilitation [4].

In order to tackle the goal of humanoid robot motion performance, which is more close to humans than today's robots, it is crucial to better understand the mechanisms and principles by which it is achieved by humans. The current stage of developments and the available biomechanical insights indicate that actuation with (variable) mechanical elasticity and damping, in combination with a proper control system, are essential to achieve human-like locomotion. Surpassing the human muscle with respect to high energy density, relatively efficient operation, scalable force, elastic energy storage, and power output will probably remain difficult for a long time [5]. In this context, an analysis of the intended bipedal motions with respect to the appropriate actuation prior to the robot's construction is of paramount importance. Omitting a thorough investigation related to the required actuation units will possibly lead to the development and selection of actuators by which the intended robot locomotion performance cannot be met.

The authors are with the Simulation, Systems Optimization and Robotics Group, Technische Universität Darmstadt, Germany.
[†] Corresponding author; phone: +49-6151-16-4811; fax: +49-6151-16-6648; e-mail: radkhah@sim.tu-darmstadt.de.
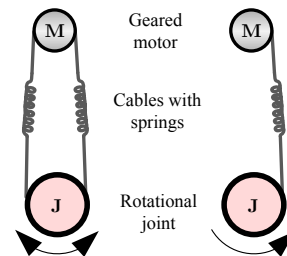
Fig. 1. Bidirectional versus unidirectional SEA (b-SEA vs. u-SEA).

In this paper, we describe the design decisions for the biologically inspired, musculoskeletal bipedal robot BioBiped1, Fig. 2(c). BioBiped1 consists of two 3-segmented legs and a simplified trunk that can tilt for- and backwards. Each leg has two rotational degrees of freedom (DoF) in the hip, for the pitch and roll movement, and one rotational DoF each in knee and ankle, for the pitch movement. It represents the first platform of a planned series, developed within the BioBiped project [6], to investigate and evaluate hypotheses and results from biomechanics by transfer to a new robot design. In accordance with the main hypothesis, that the central humanoid locomotion capability should be jogging and not walking [7], emphasis is placed on the analysis of hopping and running motions ($2 \, \mathrm{m/s}$) and the exploration of the role of muscles in the given situation. Considering a robot design with a trunk, the question addressed here is how to choose the actuation units for each of the leg joints in the sagittal plane.

An active actuation unit is comprised of a geared rotary electric direct-current (DC) motor and an elastic transmission that is coupled to a joint. The elastic transmission principle corresponds in its functionalities to that of the original Series Elastic Actuator (SEA) [8]. The advantages of series elastic actuation are well established and the resulting low-impedance control has been elaborated in many legged robots [9]. Whereas in the original SEA the gearbox is connected by a rotational spring to the joint, here it is coupled by antagonistic cables with built-in translational springs, as depicted in Fig. 1. The coupling by antagonistic cables additionally allows manual pretension of the cables. Removing one of the cables results in a solely unidirectional control of the coupled joint. In order to differentiate these two types of actuation, we introduce the notion of *bidirectional* and *unidirectional* SEA, abbreviated as b-SEA and u-SEA, in the remainder of the paper.

While actuator selection for conventionally built humanoid

robots with servo motors might appear as rather straightforward [10], it involves a host of challenges for elastic robots targeted at hopping or running motions, which require both high actuator torques and velocities. The gearing and elastic transmission enable, on the one hand, higher torques without increasing the motor size, but, on the other hand, the gearing also reduces the resulting joint velocities. Further, the elastic transmission makes tracking of a given joint trajectory more difficult and the envisaged motion control clearly affects the exploitation degree of the natural robot dynamics. So, there is a trade-off between the desired velocities, torques and efficiency of the intended motion control.

Some design possibilities are thinkable to compensate to a certain extent for undesired side effects. For instance, elastic transmissions can be built in a way, that lever arms may be modified to achieve higher joint velocities. Despite sophisticated construction options, a thorough requirement analysis prior to the actual robot construction remains necessary. A successful analysis demands suitable multibody system (MBS) dynamics models and simulations that include sufficiently accurate and realistic models of the envisaged actuators and the ground contact. Using these models, we determine the actuation requirements for a musculoskeletal robot. Based on the envisaged series elastic actuation concept, we determine step-by-step the required motor-gear units for the sagittal leg joints and subsequently compute the motor control trajectories for given reference trajectories. In order to support the findings and to increase their relevance with regard to the central project goals, the reference trajectories include aside from computer generated motions also human gait data, that were obtained from human gait experiments at the Locomotion Laboratory of Jena University [11]. The goal is not mimesis, but rather to equip the robot's legs with the necessary structures and functional properties found in the human neuro-mechanical system. At this very early stage of the project, the investigations on the mechanical system make also use of human experimental gait data to create a better basis for the evaluation of hypotheses from biomechanics and for comparisons of robot and human motion performance. As the body dynamics of the robot significantly differs from that of the human subjects, future steps will therefore include an adaptation of the reference trajectories to better exploit the robot dynamics by trajectory optimization.

In the following, we elaborate on the design criteria regarding the basic actuation of BioBiped1. Section 3 is concerned with the MBS dynamics model and simulation of BioBiped1. Subsequently, the motor-gear selection process is presented. In Section 5, the focus lies on the results obtained from investigations on hopping and human running motions. The proposed approach and obtained results are discussed in Section 6. Finally, the paper is summarized and future directions are described.

II. BASIC ACTUATION DECISIONS BASED ON THE HUMAN MUSCULOSKELETAL SYSTEM

In order to motivate the design decisions related to the actuation of BioBiped1, a good starting point would be a
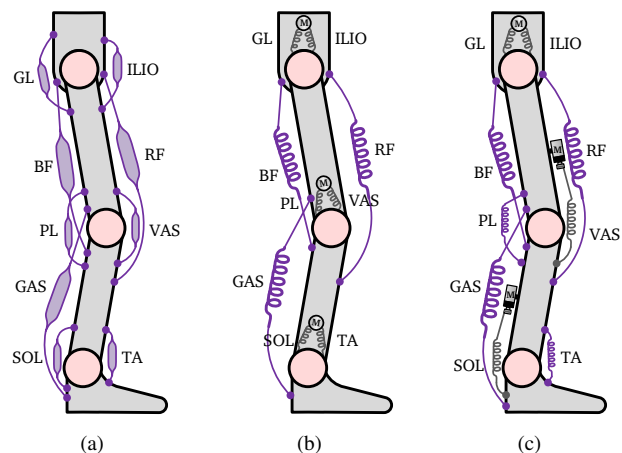
Fig. 2. Chronological evolution of the conceptualization of the actuation of BioBiped1 from left to right: (a) Essential human muscle groups during locomotion; (b) basis for the motor-gear unit selection; (c) actually constructed version of BioBiped1's actuation. Grey and purple color indicate active and passive structures, respectively.

review of the human actuation during legged locomotion, as depicted in Fig. 2(a). The muscles shown can be divided into monoarticular and biarticular, either spanning one or two joints. The monoarticular muscles appear as antagonist/agonist pairs. The hip pair is represented by *Iliacus* (ILIO), flexing the hip, and *Gluteus Maximus* (GL), extending the hip. In the knee, *Popliteus* (PL) takes on the role of flexion and *Vastus lateralis* (VAS) the role of extension. Finally, *Tibilias anterior* (TA) is responsible for flexing, aka. dorsiflexion, and *Soleus* (SOL) for extending the ankle joint, aka. plantar flexion. These monoarticular structures strongly contribute to the task of power generation during jogging [12]. In addition, the human leg has a number of biarticular muscles. The important ones are *Rectus femoris* (RF), which acts as knee extensor and hip flexor, *Biceps Femoris* (BF), which acts as knee flexor and hip extensor, and *Gastrocnemius* (GAS), which acts as ankle extensor and knee flexor. These muscles mainly transfer energy from proximal to distal joints and coordinate the synchronization of the leg joints [13]. The role and functions of these nine muscles had been previously studied in a pneumatically driven jumping monopod [14]. In the biped Lucy antagonistic pairs of pneumatic artificial muscles have been used to realize stable slow walking [15]. In the Athlete robot, which is also pneumatically driven, the anthropomorphic musculoskeletal system has been used to develop a motor command control based on human electromyographic data [16]. In [17] it has been shown that a proper selection of constant spring stiffness in the mono- and biarticular elastic structures enables walking and jogging motions even for an underactuated robot.

For targeting fast, dynamic movements with BioBiped1, an active energy supply may potentially be required for each joint in each leg, but particularly for knee and ankle joints. Thus, each joint must be capable of power generation. Consequently, during the design phase of BioBiped1, it was decided to actuate the monoarticular muscle pairs in each

joint, which resulted in the design of the b-SEA (cf. Fig. 1): The role of each of the human muscle pairs ILIO/GL, PL/VAS, and TA/SOL is mimicked by a b-SEA. This leg configuration, referred to as simulated BioBiped1, provides the basis for the motor-gear unit selection (see Fig. 2(b)). A similar bidirectional series elastic actuation for the hip and knee joints can be found in the robot TUlip [18]. In addition to the b-SEAs, the mechanical design should also allow the flexible integration of the biarticular muscles RF, BF, and GAS, as passive cables with springs (in purple). The idea is to analyze each structure's functionality through step-by-step synthesis, rather than to analyze an entire complex leg with a fixed configuration. In total, each leg can incorporate all nine relevant muscles, shown in Fig. 2(a). However, only the monoarticular muscle pairs were part of the robot leg configuration considered in the initial phase of the motor-gear unit selection process, as this musculoskeletal design introduces more complexity to the mechanical actuation system of the robot's lower body.

For the sake of completeness, we also elucidate the actuation of the built BioBiped1 robot, displayed in Fig. 2(c). Instead of b-SEAs, u-SEAs drive knee and ankle joint, i.e., only the extensor of each antagonist-agonist pair, VAS and SOL, is actuated for propelling the leg forward during jogging. The missing function of the flexors, PL and TA, is only passively integrated. This actuation difference between simulated and real robot is due to uncertainties inherent to each design phase with respect to the actual construction outcome. It results from the assumption that, considering the intended fast dynamic motions, both knee and ankle joint could be actuated by a u-SEA and its passive counterpart, instead of a b-SEA. For further information on the constructed u-SEA we refer to [7].

III. MBS DYNAMICS SIMULATION

The most realistic and reliable analysis of actuation requirements for an elastic biped prior to its actual construction presumes appropriate simulation of its dynamics. This not only includes kinematics and kinetics, but also specific actuation and, most importantly, ground contact models. For this purpose, a special multibody simulation toolbox incorporating a realistic contact model has been developed in MATLAB/Simulink [19]. Due to limited space, this section only briefly reviews the modeling and simulation of BioBiped1.

The rigid joint-link structure of BioBiped1 is displayed in Fig. 3. At the current stage of investigation, only the hip, knee and ankle joints of each leg are actuated; the rotational DoF in the trunk is fixed at the zero position. The links are modeled as cylinders of radius r and height h, which equal the length of the links based on scaled-down anthropometric data. The lengths and uniformly distributed masses of the links are listed in Fig. 3. The radii of the cylinders lie in the range of $20\,\text{mm}$ and $40\,\text{mm}$. The mass distribution with the upper body weighing 51% of the robot's total weight does not yet fully correspond to that of humans where the upper

Link Lengths	
l_{torso_width}	$150\,\text{mm}$
l_{torso_height}	$270\,\text{mm}$
l_{thigh}	$330\,\text{mm}$
l_{shank}	$330\,\text{mm}$
l_{foot_height}	$67\,\text{mm}$
l_{foot_width}	$100\,\text{mm}$

Link Masses	
m_{torso}	$4.7\,\text{kg}$
m_{thigh}	$0.9\,\text{kg}$
m_{shank}	$0.9\,\text{kg}$
m_{foot}	$0.45\,\text{kg}$
total mass	$9.2\,\text{kg}$
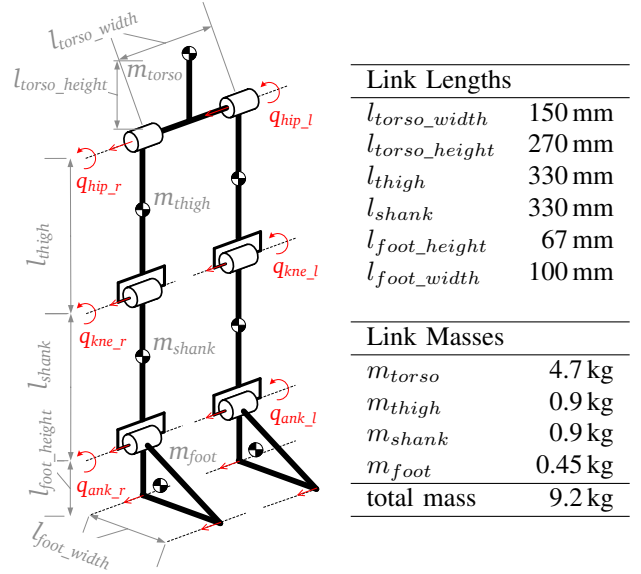
Fig. 3. Kinematic rigid joint-link structure of BioBiped1. The model is depicted in its zero position. The joint motion constraints approximately correspond to those of humans: hip pitch $[-10\,°, 50\,°]$, knee pitch $[-90\,°, 0\,°]$ and ankle pitch $[-60\,°, 20\,°]$.

body weighs about 60%. Details of the foot-ground contact model can be found in [19].

The second level of the robot description contains the actuation concept. To allow the examination of the motor currents and voltages, the motor is modeled incorporating the electrical motor dynamics. Neglecting the effect of armature inductance, the electrical dynamics of a DC motor can be described as:

$$u = R_a\, i + k_v \cdot \dot{\theta} = \frac{R_a}{k_t}\, \tau_m + k_v \cdot \dot{\theta} \qquad (1)$$

with motor angular velocity $\dot{\theta}$, input voltage u, armature resistance R_a, torque constant k_t, speed constant k_v and generated motor torque τ_m, which drives the rotor. To take into account the motor gear ratio n_g and additional transmission ratio caused by the cables n_p, a total transmission ratio z is introduced with $z = n_g\, n_p$. Friction and inertia of the gearbox are denoted as d_g and I_g, respectively. As for the gearbox efficiency, we have modeled only viscous friction and not Coulomb friction, since the latter does not play a role during fast dynamic motions. For a compact model representation, motor variables and parameters are rewritten with respect to the joint side, as *reflected variables*, based on [20]:

$$\dot{\theta}^* = \frac{1}{z}\dot{\theta} \quad \text{with} \quad |z| > 1$$

$$\tau_m^* = z \cdot \tau_m$$

$$I_m^* = z^2 \cdot (I_m + I_g)$$

$$d_m^* = z^2 \cdot (d_m + d_g)\,.$$

The link and motor equations are dynamically coupled only

through the vector of elastic torques $\boldsymbol{\tau}$:

$$\boldsymbol{\tau} = \boldsymbol{K}\left(\boldsymbol{\theta}^* - \boldsymbol{q}\right) . \tag{2}$$

$\boldsymbol{q}$ represents the measured joint positions and $\boldsymbol{K}$ is the diagonal matrix of the torsional joint stiffnesses. Due to the choice of b-SEAs with fixed lever arms for all joints (cf. Fig. 2(b)), both n_{p} and $\boldsymbol{K}$ are treated simplified as parameters with constant values. The mechanical dynamics of the motor can now be formulated as:

$$I_{\mathrm{m}}^* \, \ddot{\theta}^* + d_{\mathrm{m}}^* \, \dot{\theta}^* = \tau_{\mathrm{m}}^* - \tau \tag{3}$$

with motor inertia I_{m} and damping d_{m}. To simplify matters, reflected variables are not asterisked in the remainder of the paper.

IV. MOTOR-GEAR UNIT SELECTION PROCESS BASED ON DESIRED MOTION DATA

For investigating motor selection, the question of suitable motion trajectories for the robot arises. Desired locomotion trajectories can, for example, be either obtained from capturing human motion or computer generated. Referring to the main hypothesis of the BioBiped project, that the central humanoid locomotion ability should be jogging, the analyses regarding the actuation requirements incorporate fast dynamic motions. Hopping motion trajectories were computer generated and human running data were obtained from human gait experiments using an instrumented treadmill with force sensors and a camera system, consisting of eight high speed infrared cameras [11] (cf. Section V).

A. Determining the Motor Control Signals

The important question here is: Given desired joint angular data $\boldsymbol{q_d}(t)$ for the hip, knee, and ankle joints of each leg, what are the corresponding motor data $\boldsymbol{\theta}(t)$ and $\boldsymbol{\tau}_m(t)$, respectively? This problem can be solved by computing the inverse dynamics of the elastically actuated biped:

$$\boldsymbol{q_d}, \dot{\boldsymbol{q}}_d, \ddot{\boldsymbol{q}}_d \in \mathbb{R}^n \rightarrow \boxed{\text{INV DYN BioBiped1}} \rightarrow \boldsymbol{\tau}_m \in \mathbb{R}^n$$

The computation of the inverse dynamics of a bipedal robot with a realistic nonstiff ground contact is a difficult problem, however. For the sake of completeness, we recall the equations of motion, expressed in the Lagrangian form:

$$\boldsymbol{\tau} + \boldsymbol{\tau}_{ext} = \boldsymbol{H}(\boldsymbol{q})\ddot{\boldsymbol{q}} + \boldsymbol{C}(\boldsymbol{q}, \dot{\boldsymbol{q}}) + \boldsymbol{g}(\boldsymbol{q}) ,$$

where $\boldsymbol{q} = (q_{\mathrm{hip\_r}}, q_{\mathrm{hip\_l}}, q_{\mathrm{kne\_r}}, q_{\mathrm{kne\_l}}, q_{\mathrm{ank\_r}}, q_{\mathrm{ank\_l}})^T \in \mathbb{R}^n$. $\boldsymbol{\tau}$ is the generalized efforts vector, including the joint actuation torques, and $\boldsymbol{\tau}_{ext}$ are the torques generated by the ground contact. $\boldsymbol{H}(\boldsymbol{q})$ represents the symmetric, positive-definite joint-space inertia matrix, $\boldsymbol{C}(\boldsymbol{q}, \dot{\boldsymbol{q}})$ is the vector of centrifugal, gyroscopic, and Coriolis effects, and $\boldsymbol{g}(\boldsymbol{q})$ is the generalized gravity force vector.

To address the above question, we split up the computation of the inverse dynamics into several smaller steps without the need for actually computing directly the inverse dynamics of the elastic system. An overview is given in Fig. 4 and the steps are described in the following.

a) Step 1: Independent of the specific actuation, we first compute the forward dynamics of a rigid robot without any elasticities based on the time-varying joint reference trajectories $\boldsymbol{q}_{\mathrm{d}}(t)$. The rigid robot can be also considered as the decoupled link motion dynamics of the elastic robot whose dynamics will be computed in *Step 3*.

A classical PD controller determines the required joint torques, denoted as $\boldsymbol{\tau}_{\mathrm{st}}$, to move the rigid robot model along the desired motion trajectories, which are specified in joint coordinates, starting from measurements of the current joint states $\boldsymbol{q}_{\mathrm{st}}(t)$ during the forward dynamics computation (cf. Fig. 4). The feedback controller is designed so that the joint states $\boldsymbol{q}_{\mathrm{st}}(t)$ track the desired motion $\boldsymbol{q}_{\mathrm{d}}(t)$ as closely as possible.

The control inputs of each joint only depend on the measurement of the corresponding joint displacement and velocity. Coupling effects among joints, due to varying configuration during motion, are not considered. The forward dynamics is computed in MATLAB/Simulink using the ode45 (Dormand-Price) solver with variable step size, relative tolerance 10^{-3} and adaptive zero-crossing options. The outcomes of this step, $\boldsymbol{\tau}_{\mathrm{st}}(t)$ and $\boldsymbol{q}_{\mathrm{st}}(t)$, are used in the next step.

b) Step 2: Based on the numerical results obtained from the forward dynamics computation of the stiff robot, we compute analytically the motor angles and torques, $\boldsymbol{\theta}(t)$ and $\boldsymbol{\tau}_{\mathrm{m}}(t)$, for the elastic robot using (2) and (3). The subscript $_c$ is introduced to indicate the variables computed by this means:

$$\boldsymbol{\theta}_{\mathrm{c}}(t) = \boldsymbol{K}^{-1} \, \boldsymbol{\tau}_{\mathrm{st}}(t) + \boldsymbol{q}_{\mathrm{st}}(t) , \tag{4}$$

$$\boldsymbol{\tau}_{\mathrm{mc}}(t) = \boldsymbol{I}_{\mathrm{m}} \, \ddot{\boldsymbol{\theta}}_{\mathrm{c}}(t) + \boldsymbol{d}_{\mathrm{m}} \, \dot{\boldsymbol{\theta}}_{\mathrm{c}}(t) + \boldsymbol{\tau}_{\mathrm{st}}(t) . \tag{5}$$

It should be noted that (4) and (5) had been previously introduced to describe the equations of motion of flexible manipulators [21]. In this paper, these equations are used in a novel context for elastic bipedal robots.

c) Step 3: In this last step, the forward dynamics of the elastic robot, including its actuation, is computed. The forward dynamics simulation uses the same solver settings as in *Step 1*. Each b-SEA is controlled to track the motor positions $\boldsymbol{\theta}_{\mathrm{c}}$. The motor velocities $\dot{\boldsymbol{\theta}}_{\mathrm{c}}$ are obtained by numerical differentiation and filtering. The PD controller can be enhanced to also track the desired joint positions $\boldsymbol{q}_{\mathrm{d}}(t)$. To reduce tracking errors, the computed torques $\boldsymbol{\tau}_{\mathrm{mc}}$ are utilized as feedforward compensation (cf. Fig. 4).

The b-SEA is designed to take either voltages or torques as input variables, depending on the output of the feedback controller. To obtain rough estimates in initial investigations, it may be sufficient to feed the actuator with torques. Nevertheless, for a more reliable and useful decision on the appropriate motor-gear units the voltage input $U(t)$ is indispensable. Therefore, the PD controller also incorporates the equations of the inverse motor dynamics, as described in (1), to determine the necessary voltages. Note that in case of BioBiped1, voltage limitation is a quite critical parameter due to the pulse-width modulation which might be different for other robot platforms.
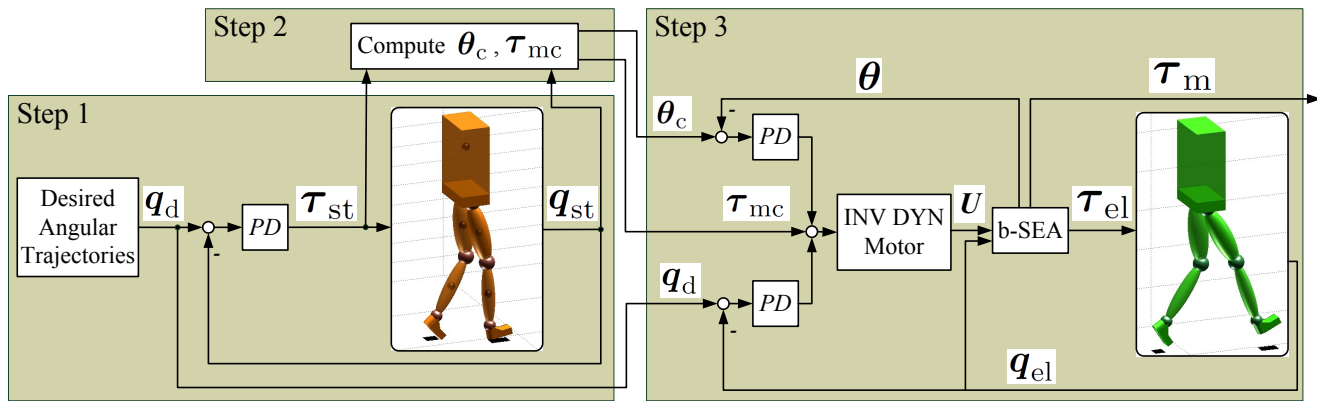
Fig. 4. Successive steps from 1 to 3 to determine the required motor control signals.

B. Preselection of the Required Actuators

A preselection of the required actuators is recommendable in order to carry out *Step 3* with approximately correct settings for the DC motor torque constant, rotor inertia, speed constant, terminal resistance and the gearbox inertia, viscous damping, and ratio. Additionally, setting the ratio, mechanical spring stiffness and viscous damping of the elastic transmission is required. The preselection depends on several factors, including the planned overall weight of the robot, electronics, and battery supply (if autonomous operation is envisaged).

Fast dynamic motions demand both high torques and velocities from the actuators. These two requirements help to determine the maximum mechanical power: $P = \dot{\theta}\,\tau_m$. By considering the most challenging phase of a jumping or running motion, we can highlight two partial requirements that need to be fulfilled by the actuators: (1) The robot must be capable of bearing its weight (static requirement) and (2) lifting its weight with a specified velocity (dynamic requirement) in the respective phase of hopping or running. Considering, in addition, the envisaged robot weight, battery supply and electronics, the findings of the above investigations allowed us decide on the RE30 Maxon motors (60 W, 24 V, Order No. 310007) with planetary reduction gearbox GP 32C with gear ratio $n_g = 66$ (Order No. 166940). In the calculations, a reduction of 20% of the level of efficiency was included preventively.

In order to choose now also the necessary range for n_p, a possibility is to set fixed maximum joint velocities/revolutions per minute (rpm) based on the desired motions, for example: 16 rpm in the hip, and 33 rpm in the knee and ankle joints. Reducing 20% of the efficiency level of the selected motor-gear unit results in the maximum velocity of 7048 rpm. In conjunction with $n_g = 66$, the desired maximum joint velocities would require approximately $n_p = 7$ for the hip and $n_p = 3$ for the knee and ankle joints. These are, however, only rough estimates for the elastic transmission ratios and may need to be further adjusted during the simulations to satisfy the torque or voltage limitations.

V. SIMULATION RESULTS

In this section we present the results obtained by performing the process described in Section IV-A. The settings of the actuation units are based on the explanations in Section IV-B and are listed in the Appendix, including controller gains and elastic transmission ratios. The selection of the spring stiffnesses was based on [11], [22] and the parameters are given in the Appendix. The torsional stiffness constants are estimated to correspond well to muscle stiffnesses during human hopping and running gaits. As postural stability and balance control will be the focus of the BioBiped project at a later stage after the complete analysis of the leg operation [7], the hopping and running motions were restricted to 1D and 2D, respectively. The results are displayed in Fig. 5, which is divided into a left and right column for the hopping and human running motions, respectively. The middle column indicates the key information for the plotted data, which is the same for both columns.

A. Hopping Motions

The desired trajectories consist of oscillations between the leg configurations $q_1 = (q_{hip}, q_{kne}, q_{ank}) = (0°, -10°, -35°)$ and $q_2 = (20°, -50°, 0°)$ (cf. Diagrams 2a, 4a, 6a of Fig. 5). The cycle time amounts to 0.32 s, resulting in the frequency 3.125 Hz, and the maximum joint velocities amount to 21 rpm for the hip, 42 rpm for the knee and 37 rpm for the ankle joint.

Diagram 1a of Fig. 5 displays the ground reaction forces (GRF). As both feet of the stiff and elastic biped touch and take off from the ground at the same time, only one foot is visible at a time. The resulting forces of both the stiff and elastic robot have the typical vertical single-humped patterns, known from humans during hopping and running, and therefore match qualitatively well.

As Diagrams 3a, 5a, and 7a of Fig. 5 indicate, motor voltage limitations are not violated. In the knee we recognize voltage saturations (Diagram 5a), but the reference motions are still tracked sufficiently well (Diagram 4a). Diagram 5a indicates that faster velocities are not feasible for the knee actuator with the current settings. The voltages U increase
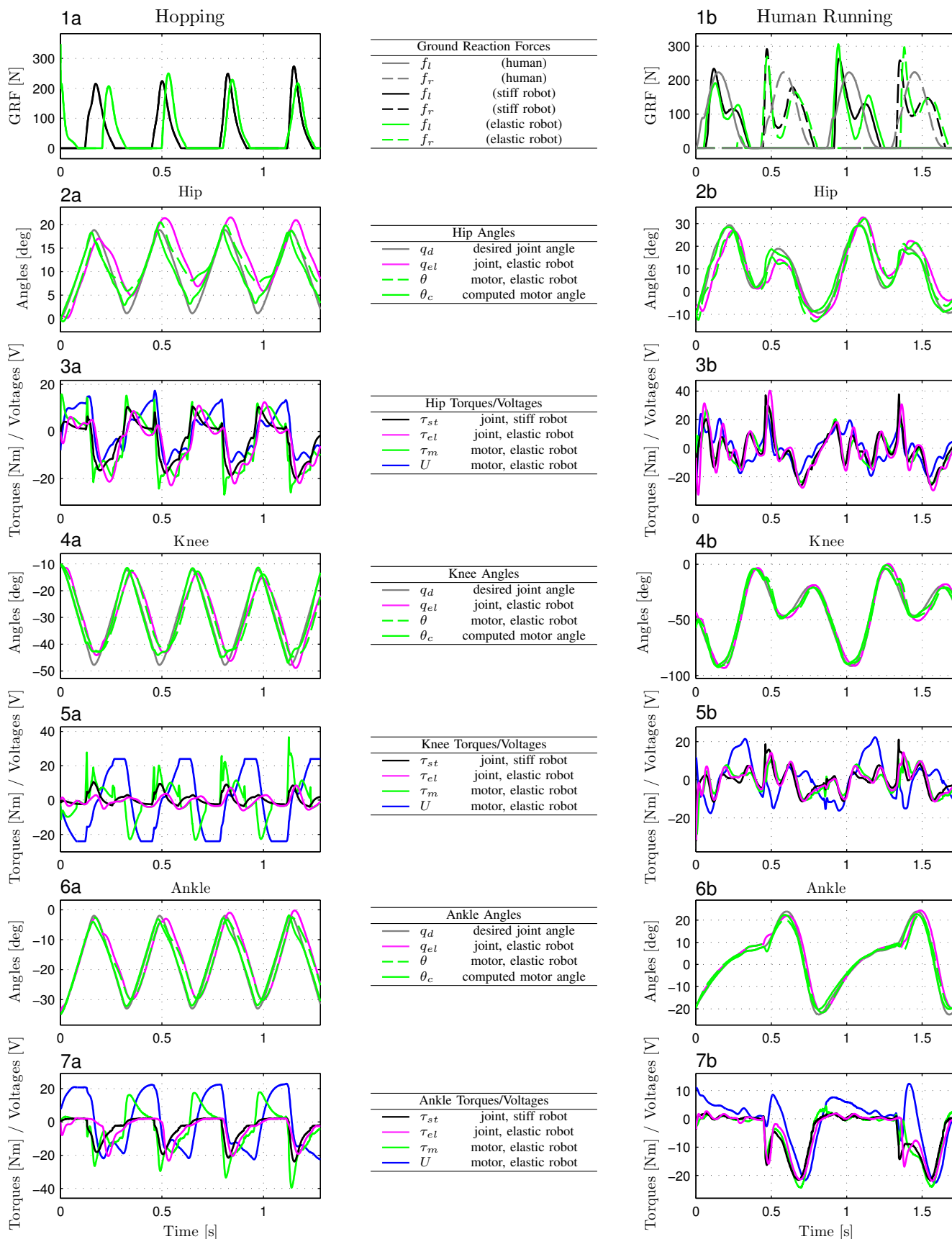
Fig. 5. The plots in left and right column display the results for the hopping and human running Trajectories, respectively. In the middle the corresponding key information for the plotted data is listed. Abbreviations used for the topmost plots: f_l refers to the left and f_r to the right foot.

with $\dot{\boldsymbol{\theta}}_{el}$ (cf. Diagrams 5a and 4a), while the torques $\boldsymbol{\tau}_{m}$ generated during the voltage peaks are comparably small. With a lower elastic transmission ratio, however, the knee joint could be moved faster, if desired. In the ankle joint, the input voltage almost reaches, but does not touch the limitations. Similar to the knee, maximum voltages $\boldsymbol{U}$ are observed during high velocities $\dot{\boldsymbol{\theta}}_{el}$. High torques $\boldsymbol{\tau}_{m}$ occur immediately before the motor turning direction is about to switch (cf. Diagrams 6a and 7a). In the hip, no saturations are detected (Diagram 2a). Similar patterns can be detected for the motor voltages $\boldsymbol{U}$ and motor torques $\boldsymbol{\tau}_{m}$, indicating that the hip motor in particular must generate high torques at low velocities.

Further, in Diagram 5a, some consecutive peaks immediately before a ground contact can be observed. This is due to the feedforward compensation term $\boldsymbol{\tau}_{mc}$ (not shown here) that prepares the motor for the impact. In order to keep torques low, it is essential to choose not too soft spring stiffnesses. Note that the current joint torques of the stiff and elastic robot, $\boldsymbol{\tau}_{st}$ and $\boldsymbol{\tau}_{el}$, should match well for almost all joints, as the stiff robot can be considered as the decoupled link motion dynamics of the elastic robot (see computation process in Section IV-A).

B. Human Running Reference Data

The analyzed running motion data consist of mean joint angles in the sagittal plane, collected from a human subject and recorded at discrete time points during a running gait cycle [11]. The running gait cycle of the human subject is characterized by cycle time 0.8621 s, step frequency 2.3209 Hz, step length 0.9052 m, and flight time 0.1120 s.

During running, the robot's GRF patterns do not exactly resemble the typical single-humped GRF patterns of the human subject, scaled to the body weight of the robot (see Diagram 1b of Fig. 5). Particularly in the first two steps illustrated, the patterns are not exactly single humped. The peak forces amount to approximately the same value as during human running. In order to eliminate the smaller hump following the first large hump in the first steps, variable-stiffness structures may need to be introduced to accommodate for ground stiffness [22].

The analyzed human running motion, as depicted in Diagrams 3b, 5b, and 7b, do not violate, nor even reach the voltage saturation. As also observed during hopping, in the hip, similar patterns for the voltages $\boldsymbol{U}$ and torques $\boldsymbol{\tau}_{m}$ can be detected, which again indicates that the hip actuator needs to be capable of generating high torques.

C. Attached Video

The attached video contains animations of the hopping and running motions that are displayed in Fig. 5. Animations are presented for both stiff and elastic robot in real-time and $0.25\times$ real-time.

VI. DISCUSSION

The results obtained indicate that the used motor-gear combinations and elastic transmissions are capable of tracking the designed motions without violating the maximum voltages. We were aiming at running motions with moderate speed (2 m/s), clear flight phases and ground clearance. From the simulation results obtained, we can expect an accordingly constructed robot to perform equally well. In real experiments, BioBiped1 turned out to be capable of both synchronous two-legged and alternating hopping motions with flight phases of 200 ms and ground clearance of 5 cm (see videos on the project website [6]), although the monoarticular b-SEA in knee and ankle joints had been realized in a slightly different manner. This actuation difference between simulated and real robot necessitates to identify the exact relations of a b-SEA and a u-SEA in conjunction with a passive structure. The proposed approach does not loose its generality as the actuator differences can be taken into account during modeling.

Due to the different geometric joint configuration and frequencies characterizing the hopping and running motions, slightly different spring stiffnesses and elastic transmission ratios had to be chosen to satisfy the motor voltage limitations (see the Appendix). These settings should be adapted on-line in case of gait transitions. There is already much research into on-line adaptable compliance mechanisms and such mechanisms will be considered at a later project stage.

A main focus of future work will be placed on the interplay of all series elastic structures requiring an optimization study that incorporates low active actuation requirements. Although not yet thoroughly analyzed, it can be stated, that lower spring stiffnesses would have immensely increased the demands on the actuators.

Experiments are necessary to analyze the motions tested here on the real robot, which requires a parameter identification beforehand to ensure that the simulated robot's behavior meets the real one's. The used link masses and lengths were initially planned values that approximately match BioBiped1. Link inertias were estimated according to the planned geometry of the links.

A final remark should be made concerning the selection of identical motor-gear units for all joints of BioBiped1, although, in humans, not all joints require the same power. This is due to several reasons. BioBiped1 is just the first prototype within a planned series and many questions are still open. For the motions that were tested here, quite dynamic actuator activities could be observed in almost each joint during the entire simulation time. Besides, due to the possibility to exchange springs and set different lever arms, each joint is actually driven by a different actuation unit despite identical motor-gear units. Furthermore, an overall control concept fitting the mechanical design of BioBiped1 is still to be investigated. Different motor-gear units would have complicated the construction of the real BioBiped1 and, most importantly, the access to insights.

VII. CONCLUSIONS AND FUTURE WORKS

In this paper, we have described design decisions for a musculoskeletal robot and have proposed an approach to

determine the actuation requirements for a given motion. The equations used are well established in robotic manipulation, but here they are embedded into a step-by-step process to compute the control signals for the actuators of an elastic biped that is electrically driven and expected to perform highly dynamic gaits. This method is applicable to any other robot with series elastic actuation as well. In addition, it can be even considered as a workaround for the control of a bipedal robot whose sophisticated mechanics still needs to be integrated into an overall control concept. As next steps, parameter estimation techniques and trajectory optimization will be applied to fit the simulation model even closer to the experimental performance of BioBiped1 robot and to better utilize the robot's specific dynamic properties. Also, the motor control signals obtained will be applied to test and analyze how well the real BioBiped1 performs the hopping and running motions.

APPENDIX

Settings for the results presented in Section V are listed in Table I.

TABLE I
PARAMETERS USED IN THE SIMULATIONS

Geared DC motor in hip, knee, ankle	
motor torque constant: $k_{\mathrm{t}} = 2.6 \cdot 10^{(-2)} \, \mathrm{Nm/A}$	
motor rotor inertia: $I_{\mathrm{m}} = 3.3 \cdot 10^{(-6)} \, \mathrm{kg \, m^2}$	
motor speed constant: $k_{\mathrm{v}} = 2.6 \cdot 10^{(-2)} \, \mathrm{Vs/rad}$	
motor armature resistance: $R_{\mathrm{a}} = 0.611 \, \mathrm{Ohm}$	
gearbox ratio: $n_g = 66$	
gearbox inertia: $I_{\mathrm{g}} = 7 \cdot 10^{(-8)} \, \mathrm{kg \, m^2}$	
gearbox viscuos damping: $d_{\mathrm{v}} = 10^{(-5)} \, \mathrm{Nms/rad}$	
Simulation setup	
Hopping	Running
Elastic transmissions	
viscuos damping in hip, knee, ankle: $d_{\mathrm{e}} = 0.05 \, \mathrm{Nms/rad}$	
ratio in hip, knee, ankle: $n_p = 3$	ratio in hip, ankle: $n_p = 2$ ratio in knee: $n_p = 1$
spring stiffness hip: $260 \, \mathrm{Nm/rad}$ spring stiffness knee: $100 \, \mathrm{Nm/rad}$ spring stiffness ankle: $290 \, \mathrm{Nm/rad}$	spring stiffness hip: $280 \, \mathrm{Nm/rad}$ spring stiffness knee: $130 \, \mathrm{Nm/rad}$ spring stiffness ankle: $250 \, \mathrm{Nm/rad}$
Joint controller gains of stiff robot	
P-gain hip: $k_p = 200$ P-gain knee: $k_p = 60$ P-gain ankle: $k_p = 200$ D-gain hip: $k_d = 50$ D-gain knee: $k_d = 13$ D-gain ankle: $k_d = 50$	P-gain hip: $k_p = 200$ P-gain knee: $k_p = 60$ P-gain ankle: $k_p = 200$ D-gain hip: $k_d = 50$ D-gain knee: $k_d = 13$ D-gain ankle: $k_d = 50$
Motor controller gains of elastic robot	
P-gain hip, knee, ankle: $k_p = 32$ D-gain hip, knee, ankle: $k_d = 5$	P-gain hip, knee, ankle: $k_p = 16$ D-gain hip, knee, ankle: $k_d = 2$

ACKNOWLEDGMENTS

REFERENCES

[1] J. M. Hollerbach, I. W. Hunter, and J. Ballantyne, "A comparative analysis of actuator technologies for robotics." MIT Press, 1992, pp. 299–342.

[2] M. Zinn, O. Khatib, B. Roth, and J. K. Salisbury, "Actuation methods for human-centered robotics and associated control challenges," in *Springer Tracts in Advanced Robotics*. Springer, 2003, vol. 4, ch. Control Problems in Robotics.

[3] R. V. Ham, T. Sugar, B. Vanderborght, K. Hollander, and D. Lefeber, "Compliant actuator designs," *IEEE Robot. Automat. Mag.*, vol. 16, no. 3, pp. 81–94, 2009.

[4] Viactors. [Online]. Available: http://www.viactors.eu

[5] J. D. Madden, "Mobile robots: Motor challenges and materials solutions," *Science*, vol. 318, no. 5853, pp. 1094–1097, 2007.

[6] Biobiped project website. [Online]. Available: www.biobiped.de

[7] K. Radkhah, C. Maufroy, M. Maus, D. Scholz, A. Seyfarth, and O. von Stryk, "Concept and design of the BioBiped1 robot for human-like walking and running," *Special Issue on "Advances on Humanoid Robot Body-ware Design and Development" in International Journal of Humanoid Robotics*, 2011, in press.

[8] G. A. Pratt and M. M. Williamson, "Series elastic actuators," in *IEEE International Workshop on Intelligent Robots and Systems*, 1995, pp. 399–406.

[9] G. A. Pratt, "Low impedance walking robot," *Integ. and Comp. Biol.*, vol. 42, pp. 174–181, 2002.

[10] D. Wollherr, M. Hardt, M. Buss, and O. von Stryk, "Actuator selection and hardware realization of a small and fast-moving autonomous humanoid robot," in *IEEE/RSJ International Conference on Intelligent Robots and Systems*, 2002, pp. 2491–2496.

[11] S. Lipfert, "Kinematic and dynamic similarities between walking and running," Ph.D. dissertation, Friedrich-Schiller-Universität, Jena, Germany, 2009.

[12] L. Grègoire, H. E. Veeger, P. A. Huijing, and G. J. van Ingen Schenau, "Role of mono- and biarticular muscles in explosive movements," *International Journal of Sports Medicine*, vol. 5, pp. 301–305, 1984.

[13] R. Jacobs, M. F. Bobbert, and G. J. van Ingen Schenau, "Mechanical output from individual muscles during explosive leg extensions: The role of biarticular muscles," *Journal of Biomechanics*, vol. 29, no. 4, pp. 513–523, Apr. 1996.

[14] K. Hosoda, Y. Sakaguchi, H. Takayama, and T. Takumai, "Pneumatic-driven jumping robot with anthropomorphic muscular skeleton structure," *Autonomous Robots*, vol. 28, no. 3, pp. 307–316, 2010.

[15] B. Verrelst, R. V. Ham, B. Vanderborght, F. Daerden, D. Lefeber, and J. Vermeulen, "The pneumatic biped "Lucy" actuated with pleated pneumatic artificial muscles," *Autonomous Robots*, vol. 18, no. 2, pp. 201–213, 2005.

[16] R. Niiyama, S. Nishikawa, and Y. Kuniyoshi, "Athlete robot with applied human muscle activation patterns for bipedal running," in *IEEE-RAS International Conference on Humanoid Robots*, 2010.

[17] A. Seyfarth, R. Tausch, M. Stelzer, F. Iida, A. Karguth, and O. von Stryk, "Towards bipedal jogging as a natural result for optimizing walking speed for passively compliant three-segmented legs," *The International Journal of Robotics Research*, vol. 28, no. 2, pp. 257–265, 2009.

[18] D. Hobbelen, T. de Boer, and M. Wisse, "System overview of bipedal robots Flame and TUlip: tailor-made for Limit Cycle Walking," in *IEEE/RSJ International Conference on Intelligent Robots and Systems*, 2008, pp. 2486–2491.

[19] T. Lens, K. Radkhah, and O. von Stryk, "Simulation of dynamics and realistic contact forces for manipulators and legged robots with high joint elasticity," in *International Conference on Advanced Robotics*, 2011, pp. 34–41.

[20] T. Lens, J. Kunz, and O. von Stryk, "Dynamic modeling of the 4 DoF BioRob series elastic robot arm for simulation and control," in *SIMPAR*, ser. Lecture Notes in AI, vol. 6472. Springer, 2010, pp. 411–422.

[21] A. D. Luca, "Feedforward/feedback laws for the control of flexible robots," in *IEEE International Conference on Robotics and Automation*, 2000, pp. 233 –239.

[22] C. Farley and D. Morgenroth, "Leg stiffness primarily depends on ankle stiffness during human hopping," *Journal of Biomechanics*, vol. 32, pp. 267–273, 1999.